A Synergistic Dual-Functional Silver-Manganese Dioxide-CNTs Ternary Composite Electrocatalyst for Solid-State Zinc-Air Battery

Guoqing Zhang *, Tuanwu Cao , Peng Zhang , Shuying Kong , Binbin Jin

Posted Date: 3 January 2024

doi: 10.20944/preprints202401.0200.v1

Keywords: Electrocatalyst; Oxygen reduction reaction; Air electrode; Electrocatalytic activity; Solid-state zinc-air battery

Article

A Synergistic Dual-Functional Silver-Manganese Dioxide-CNTs Ternary Composite Electrocatalyst for Solid-State Zinc-Air Battery

Guoqing Zhang [1,*], Tuanwu Cao [1], Peng Zhang [2], Shuying Kong [1], Binbin Jin [1]

[1] Chongqing Key Laboratory of Inorganic Special Functional Materials, Yangtze Normal University, 16 Juxian Road, Fuling, Chongqing, China

[2] College of Materials Science and Engineering, Yangtze Normal University, 16 Juxian Road, Fuling, Chongqing, China

* Correspondence: yzhanggq@163.com

Abstract: Exploring effective oxygen reduction reaction (ORR) electrocatalysts is crucial for progress in solid-state alkaline zinc-air batteries (ZAB). In this paper, silver-manganese dioxide-carbon nanotubes (SMC) ternary composites, which function as Electrocatalyst for air Electrodes, was produced via the pyrolysis of silver permanganate under microwave irradiation in one step. A scanning electron microscope (SEM), X-ray diffraction (XRD), and an energy dispersion spectrometer (EDS) have consistently determined that SMC consists of silver and alpha-manganese dioxide, which anchored on the surface of CNTs. Through polarization and chronoamperometery curves, the electrocatalytic activity of SMC for ORR was examined. The results reveal that SMC has higher catalytic activity than the chemically produced electrocatalyst for ORR in alkaline condition. Finally, a solid-state zinc-air cell with an electrocatalyst was constructed and tested. Constant current discharge curve of the zinc-air cell with SMC has a long discharge voltage plateau and a 60.03 mAh capacity at 30 $mA{\cdot}cm^{-2}$. The mechanism of improvement in electrocatalytic activity was also discussed. In a summary, the strategy described in this study and the electrocatalyst produced can be regarded as an effective method for making a robust oxygen reduction catalyst toward solid-state zinc-air batteries.

Keywords: electrocatalyst; oxygen reduction reaction; air electrode; electrocatalytic activity; solid-state zinc-air battery

1. Introduction

Alkaline zinc-air battery (ZAB) is one of the latest technology in the battery field, and is known as "green energy for the 21st century". Generally, the energy of a battery is stored in its two electrode materials, while ZABs are different. Only the anode, namely the zinc electrode, stores energy. The air electrode is a tool for energy conversion; its active material comes from the surrounding air. From energy storage and conversion point of view, therefore, ZAB is both an energy storage tool and a fuel cell. Based on these characteristics, it has advantages of a high specific energy (theoretical specific energy of 1350 $Wh{\cdot}kg^{-1}$[1–3]), stable working voltage, cheap raw materials and environmentally friendliness. However, due to the low discharge current of ZAB and the expensive precious metals catalyst, its market and application range are limited. In light of the aforementioned issues, substantial research on electrocatalysts for ORR has been conducted[4–6]. There are roughly the following categories: (i) Carbon was first used as an electrocatalyst for ORR, but its catalytic activity was quite low[7,8]. (ii) So far, precious platinum is the most studied electrocatalyst with the best catalytic activity and stability. However, its expensive makes it difficult to achieve large-scale application[8,9]. (iii) Pt-free transition metal chelate, unprecise metal oxides and metal alloys as air electrode catalysts[10–12], among which silver and manganese oxide are the most studied[13,14].

As to the reason of low discharge current of ZAB, Yeager et al[15] proposed that the discharge intermediate product of harmful HO_2^- primarily causes the high polarization of air electrode except other resistances. One method for reducing the polarization of the air electrode is to use a variety

 doi:10.20944/preprints202401.0200.v1

of carbon compounds as the catalyst support. Carbon nanotubes (CNTs) have shown remarkable structural, mechanical, and electrical properties, making them suitable for use in field emitters, nanoelectronic devices, nanotube-reinforced materials, and SPE probe tips[16,17]. CNTs, in particular, are being considered as potential supports for heterogeneous catalysts[18]. Another approach is to choose multifunctional catalysts such as metal silver, manganese dioxide, and various metal alloys[19–22].

The traditional method for synthesizing catalysts is chemical reducing, which has numerous drawbacks such as long reaction times, low output, and so on. In the synthesis of inorganic materials, microwave procedures are for the most part known to be quicker and more straightforward than regular strategies[23]. Heat is generated internally rather than from external sources during microwave heating, resulting in nearly 100% conversion of electromagnetic energy to heat. Energy is rapidly adapted and used in the interaction of microwaves with matter. Other benefits include reduced waitting time, energy savings, faster heating rates, improved mechanical properties, and environmental friendliness. It is expected that the use of microwave heating will enable a novel method of preparing electrocatalyst for air electrodes.

In this study, silver permanganate, a precursor for the catalyst, was heated using microwave irradiation to create dual-functional catalysts that combine silver and manganese dioxide. Silver permanganate is easily decomposited, and the products may be uniformly deposited onto CNTs. The fine silver particles and manganese dioxide formed when silver permanganate is heated can both be simultaneously deposited on CNTs. Through electrochemical testing in an alkaline environment, the catalytic activity of the air electrodes using dual-functional silver-manganese dioxide anchored on CNTs was examined.

2. Results and Discussion

2.1. Morphology and composition analysis

SEM analysis of the morphology of the as-prepared m-SMC is shown in Figure 1. The CNTs have an extremely lengthy and present a profoundly ensnared network structure displayed in Figure 1(a). The catalyst m-SMC SEM micrograph revealed a well-defined, nanoscale cuboidal-shaped particles. From Figure 1(b), we can see that catalyst powders, i.e., silver and manganese dioxide particles are difficult to distinguish. And m-SMC powders are more supported uniformly on the CNTs network. So, we can enunciate that the m-SMC displays an interwoven fibrous structure. The uniform dispersion and interwoven structure can offer a closely contact between catalyst powers and CNTs, which are beneficial for particle-to-particle electronic interaction between silver and manganese dioxide via CNTs[24]. For air electrode, such this catalyst structure will enable closely contact between oxygen, catalyst powders and electrolyte three-phrase interface. And the gas oxygen entered in air electrode can be electrochemically reduction smoothly.

To investigate the composition of m-SMC catalyst, EDS analysis were carried out. One can see that the Mn, O, Ag and C peaks are observed in the EDX spectrum of the m-SMC composite, confirming the presence of silver, manganese dioxide and CNTs. The peak around 2.97 keV shows the presence of silver. As illustrated in Figure 2, carbon, oxygen, silver, and manganese were all detected. Their atom concentrations in m-SMC are also shown in the figure.

Preprints (www.preprints.org) | NOT PEER-REVIEWED | Posted: 3 January 2024 doi:10.20944/preprints202401.0200.v1

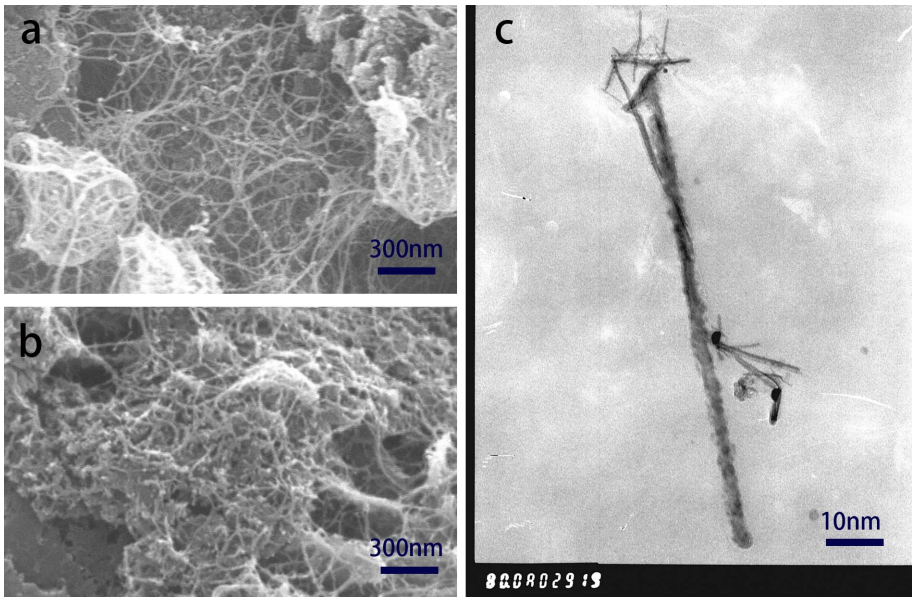

Figure 1. Typical SEM images of the CNTs (a), m-SMC (b), and TEM image of m-SMC (c).

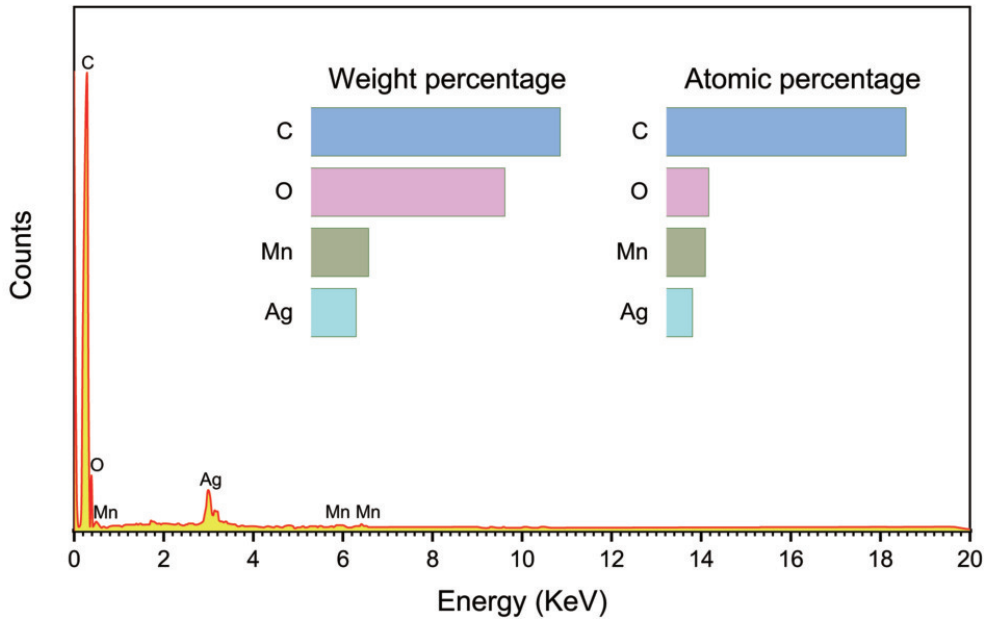

Figure 2. Energy dispersion spectrometer (EDS) analysis of m-SMC catalyst.

The crystalline nature and phase characteristics of m-SMC was studied by using XRD in a 2-theta range of 10°- 80° at 0.02 °/s scan rate. Figure 3 shows the diffraction pattern of m-SMC. Peaks at 2-theta of 38.11°, 44.29°, 64.44°, 77.39°, corresponding to the (1 1 1), (2 0 0), (2 2 0), (3 1 1) crystalline planes of silver, respectively. Peaks at 2-theta of 28.84°, 36.69°, 41.97°, 49.86°, 60.27°, 65.10°, 71.19°, 78.58°, corresponding to the (3 1 0), (4 0 0), (3 0 1), (4 1 1), (5 2 1), (0 0 2), (2 2 2), (3 3 2) crystalline planes of alpha manganese dioxide. As a result, the majority of diffraction peaks coincide with the standard values of tetragonal-MnO_2 (JCPDS 44-0141) and space group 14/m 87[25]. The strong intensity of peaks locating at 2-thata of 77.39° and 64.44° attribute to overlying of two peaks (one is [3 3 2] of α-MnO_2; another is [3 1 1] of silver). Average crystallite size of m-SMC was calculated via Scherer method (eq.3).

$$D = \frac{K\lambda}{\beta \cos\theta} \tag{1}$$

Preprints (www.preprints.org) | NOT PEER-REVIEWED | Posted: 3 January 2024 doi:10.20944/preprints202401.0200.v1

where D, K and λ, θ, β were average crystallite size, full width half maximum, and wavelength, scattering angle, shape factor with value of 0.9, respectively. The average crystallite size of m-SMC was 3.49 nm.

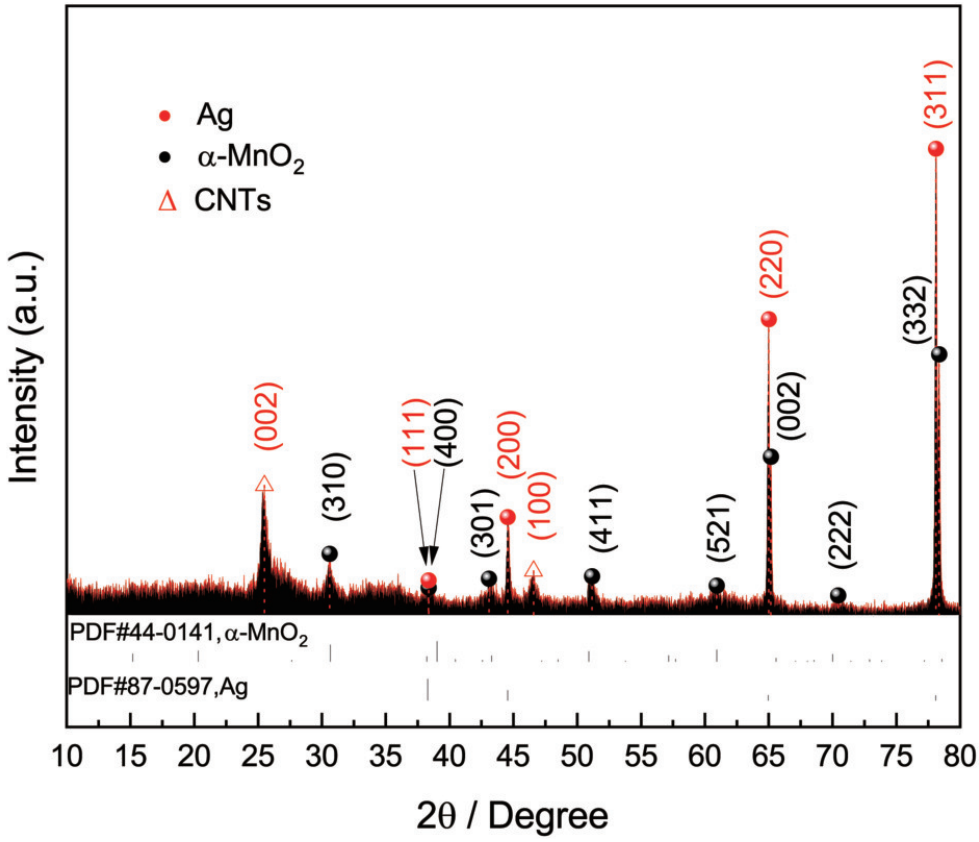

Figure 3. XRD pattern of m-SMC catalyst.

2.2. Polarization characteristics of the air electrode

During oxygen reduction at m-SMC catalyzed air electrode, the roles of silver and manganese dioxide are different. Silver facilitates the direct reduction of O_2 to $4OH^-$[26–28], and also the HO_2^- anion disproportionation[29], while manganese dioxide can't take part in the $4e^-$ reduction of O_2 to $4OH^-$[30], this $4e^-$ reduction process can be expressed by equation (4).

$$O_2 + 2H_2O + 4e^- \rightarrow 4OH^- \tag{2}$$

In this $4e^-$ process, those oxygen atoms that are not reduced to OH^- may be reduced to peroxide (HO_2^-) in a two electron, the reaction can be described as:

$$O_2 + H_2O + 2e^- \rightarrow HO_2^- + OH^- \tag{3}$$

$$HO_2^- \rightarrow O_2 + 2OH^- \tag{4}$$

In contrast to the $4e^-$ reduction process(equation (4)), the two-electron reduction path (equation (5)) involves peroxide species. Due to its high oxidizability, the peroxide buildup poisons the catalysts or carbon support materials as well as reduces ORR catalysis efficiency[26,31,32]. Peroxide HO_2^- is very poisonous to air electrode, so it is greatly imperative to eliminate peroxide. Recently, Y.L. Cao, et al[33] proposed a mechanism of oxygen reduction at MnO_2-catalyzed air electrode, according to the mechanism, those oxygen atoms that are not reduced to OH^- might be reduced through chemical

Preprints (www.preprints.org) | NOT PEER-REVIEWED | Posted: 3 January 2024 doi:10.20944/preprints202401.0200.v1

oxidation of the surface Mn^{3+} ions created by the discharge of MnO_2, consequently, the production of peroxide might be restrained. α-MnO_2 generally shows the better ORR performance because of its large tunnel structure, which makes ion move easy in the lattice framework[34,35]. The mechanism is described as follows:

$$MnO_2 + H_2O + e^- \leftrightarrow MnOOH + OH^- \quad (5)$$

$$2MnOOH + O_2 \leftrightarrow 2(MnOOH \cdot O^-) \quad (6)$$

$$MnOOH \cdot O^- \leftrightarrow MnO_2 + OH^- \quad (7)$$

Based on the above-mentioned ORR mechanism analysis, the final catalytic effectiveness of MnO_2 equals to $4e^-$ reduction reaction of oxygen (equation 4). Therefore, silver and manganese dioxide included in the m-SMC have synergistic catalytic activity in the same direction[32], i.e., m-SMC posses a dual function toward ORR.

Figure 4 shows the liner voltammograms recorded at an air electrode with m-SMC. As an examination, the cv curve of the air electrode with c-SMC is likewise given in the figure. The cathodic currents for the air electrodes begin to emerge around -0.005 V, however, as the potential becomes more negative, the cathodic current for the m-SMC electrode increases rapidly, whereas the cathodic current for the c-SMC catalyzed air electrode increases very slowly. Clearly, the m-SMC has higher cathodic current than that of c-SMC, showing an improved electrocatalytic activity of m-SMC for ORR. The distinction in polarization feature of the two cathodes with catalysts made by different strategies ought to emerge from the level of scattering of catalysts particles. Under microwave irradiation, catalyst particles scattered consistently onto CNTs, which prompts more opportunity to intently each other between catalyst powders and oxygen molecules, while oxygen reduction happens effectively and quickly.

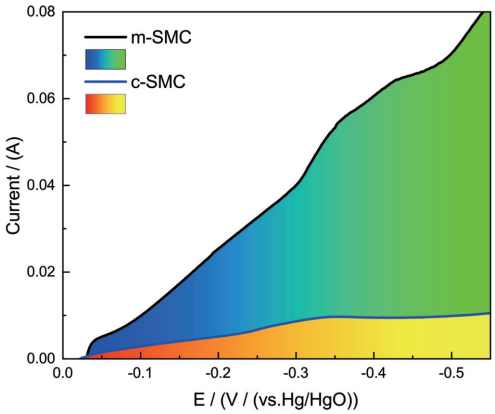

Figure 4. Linear voltammograms of air electrodes with the catalysts, m-SMC (a), c-SMC (b)

2.3. Chronoamperometry measurements

Figure 5 shows the chronnamperometries for air electrodes with SMC catalyst. The chronoamperometery method involves applying a potential jump on the electrode from rest potential to a negative potential and recording the current transient. The figure demonstrates that the two air electrodes' cathodic currents at a potential of 0.3 V all decrease sharply within 0.1 s before stabilizing. Notwithstanding, the values of cathodic current are very unique. The cathodic current of the air electrode with m-SMC is 0.1 A higher than that of the air electrode with c-SMC. This result further confirmed the m-SMC catalyst made by microwave irradiation having a good catalytic activity.

Preprints (www.preprints.org) | NOT PEER-REVIEWED | Posted: 3 January 2024 doi:10.20944/preprints202401.0200.v1

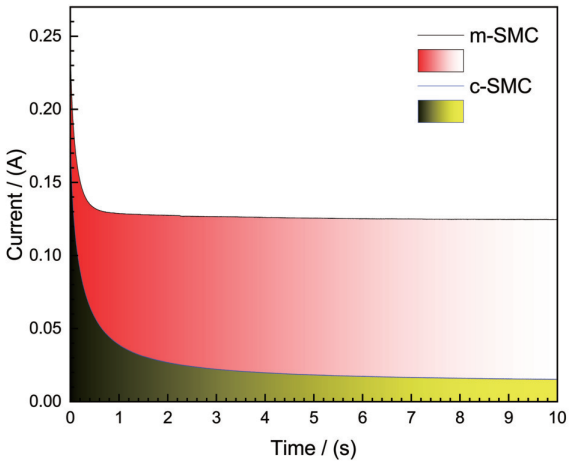

Figure 5. Chronnamperogram curves of air electrodes with the catalysts, m-SMC (a), c-SMC (b)

2.4. Electrochemical impedance spectroscopy (EIS) study

Typical electrochemical impedance spectrum of zinc-air cells with catalysts are shown in Figure 6, in which Nyquist and Bode plot (insert) are also presented. The axis of x and y address the real part (Z') and the imaginary part of the impedance (Z"). By and large, the impedance spectrum are depressed semicircles in the complex plane and they do not show the "semicircle focused on the real axis" highlight that is commonly seen in systems that can be represented by a simple resistance-capacitance (RQ) equivalent circuit. The origin of this deviation can be ascribed to the presence of inhomogeneous and porosity upon the electrode surface, which gives rise to a frequency-dependent penetration depth for the ac wave. At a high frequency region (f $>$ 1 kHz), besides induction, the Nyquist plot is composed of a small depressed semicircle and Bode plot has a wave peak indicating the presence of reactance, which is generated by the ohm polarization of the air electrode; at the intermediate frequency region (10 Hz $<$ f $<$1 kHz), the semicircle is caused by the electrochemical polarization of the air electrode; at low frequency (f $<$10 Hz), the plot has a tendency to change to a straight line with an angle of 45^o, which is a characteristic of the semi-finite diffusion (Warburg impedance Z_w). The electrolyte resistance is determined by the point of intersection of the high-frequency semicircle with the real axis[36,37].

In Figure 6, the equivalent circuit represents the structure of the measured system and some actually kinetic parameters, in which, L is the inductance, R_1 is the electrolyte resistance between the electrode surface and the reference electrode, R_2 is the surface contact resistance between the electrode and electrolyte addition to the ohm resistance of the air electrode, CPE_1 and CPE_2 represent constant phase elements (CPE) caused by electrode roughness or by inhomogeneous reaction rates on the electrode surface, R_3 is the electrochemical polarization resistance, and Z_w is the Warburg impedance. The calculated kinetic parameters for air electrodes are given in Table 1. From this table, it is clear that the distinction of electrolyte resistance (R_1) is very tiny for two air electrodes, while ohm resistance addition to interface resistance (R_2) and electrochemical polarization resistance (R_3) are obviously different. Specially, m-SMC-catalyzed air electrode has lower values of R_2, R_3 and Z_w than that of the c-SMC-catalyzed air electrode. So, it can be concluded that employing m-SMC as catalyst can reduce R_2 and R_3, i.e., m-SMC is favorable to the oxygen reduction reaction. The explanation might be ascribed to the high surface area, extraordinary surfacial morphology and intently contact of the material.

Preprints (www.preprints.org) | NOT PEER-REVIEWED | Posted: 3 January 2024 doi:10.20944/preprints202401.0200.v1

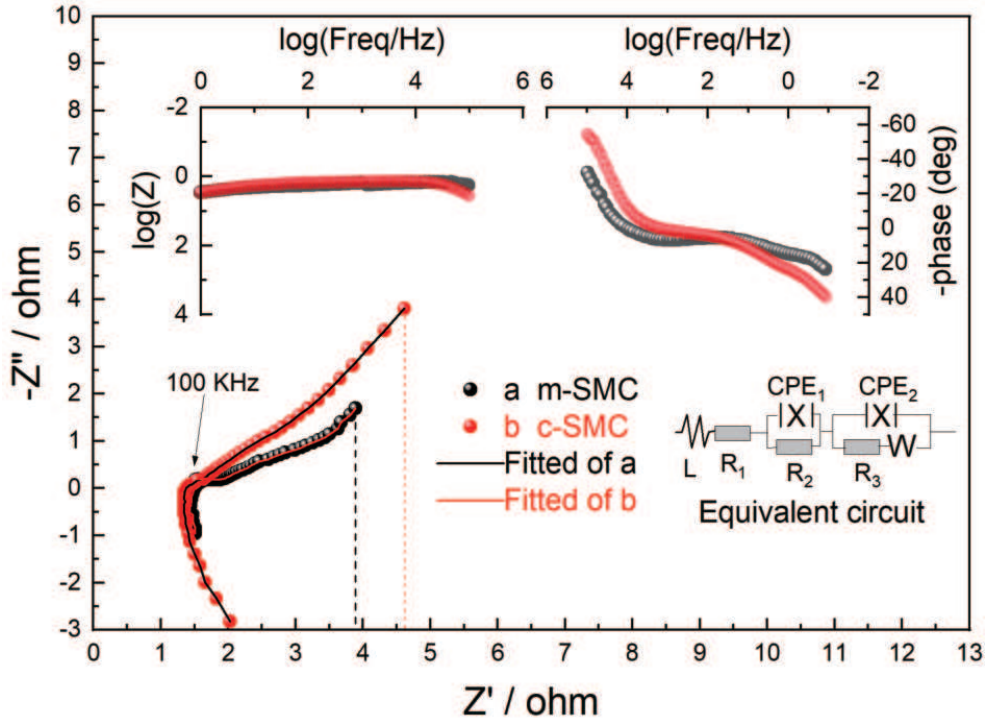

Figure 6. EIS of the zinc-air cells with catalysts, m-SMC (a) and c-SMC (b)

Table 1. Table 1 Electrode kinetic parameters fitted with equivalent circuit

Air electrode	L (H)	R1 (Ω)	R2 (Ω)	Q1 Y_0, n	Q2 Y_0, n	R3 (Ω)	W (Ω)
c-SMC	$0.2781e^{-5}$	1.369	0.617	$0.5057e^{-3}$ n=0.6333	0.1357 n=0.7546	1.2011	1.635
m-SMC	$0.9467e^{-6}$	1.447	0.2001	$0.8152e^{-3}$ n=0.8304	$0.2185e^{-1}$ n=0.8075	0.0903	0.1427

2.5. Galvanostatic discharge measurements

Figure 7 shows the discharge curves of all solid zinc-air cells with catalysts at a high constant current of 94.2 mA(30 mA·cm^{-2}). During the discharge of the cell, zinc converses from simple substance to zinc oxide, while oxygen from the air is electrochemically reduced at the cathode.

At a high constant current drain of 94.2 mA for the cells with 0.03 g catalysts come from different strategies and 0.5 g zinc powder. From Figure 7, we can see that the cells can support the current drain at about 1.0 V, and the discharge curves is smooth. Discharge time of the cell can be lasted for 20 min (1038.82 mAh·g^{-1} based on the mass of catalyst) and 25 min (1287.68 mAh·g^{-1}), respectively. It is showed that the discharge capacities of the cells were insubordinately different, which might be ascribed the more uniform dispersion and interwoven structure of m-SMC catalyst. This structure of catalysts strengthens the catalytic activity, and boosts the rate of oxygen reduction. The superiority is clear with m-SMC catalyst compared to c-SMC at their eletrocatalytical activity. This has been true in case of m-SMC where covalent interactions because of proximity of Ag to MnO_2 lead to improved catalytic activity[24]. The result further confirm that microwave heating is worth accepting to synthesis silver-manganese dioxide-CNTs ternary composite catalyst, are also in agreement with the results of morphology and polarization.

Preprints (www.preprints.org) | NOT PEER-REVIEWED | Posted: 3 January 2024 doi:10.20944/preprints202401.0200.v1

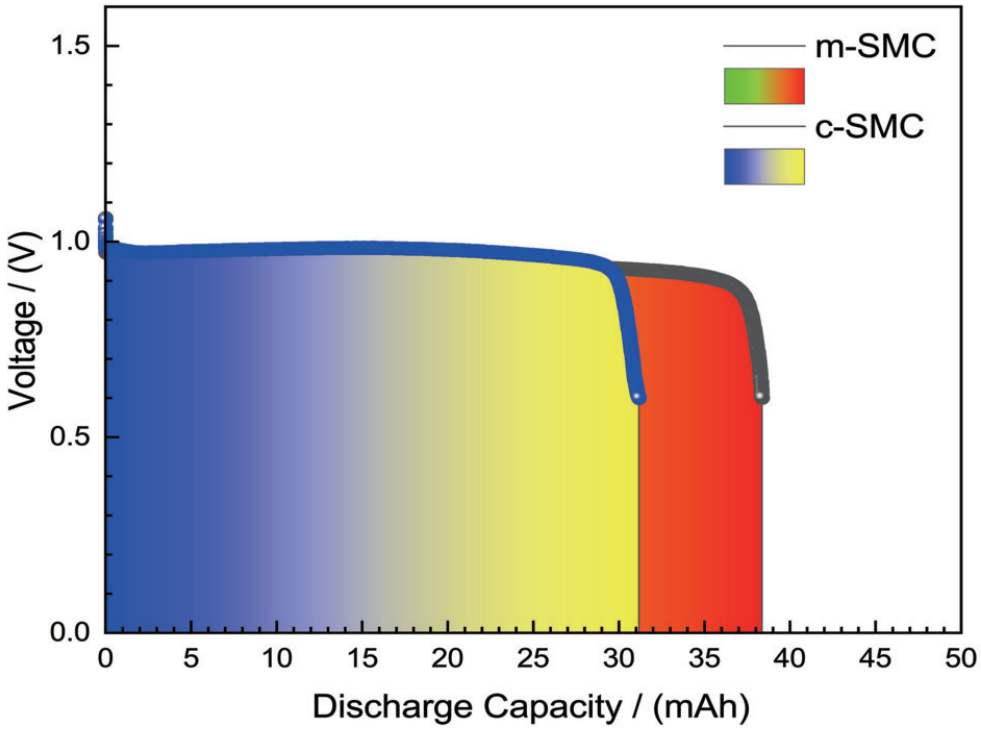

Figure 7. Discharge curves of the solid-state zinc-air cells with catalysts, m-SMC (a) and c-SMC (b), at 94.2 mA

3. Materials and Methods

3.1. Preparation of Catalysts

CNTs were purchased from TANFENG, Corporation. Silver permanganate were purchased from Aldrich. Dissolving 13.05 mg of silver permanganate in 50 mL of distilled water at 25 °C resulted in a rich purple solution. After that, 100 mg of CNTs were dispersed into this silver permanganate aqueous solution. The mixture was then placed in a microwave oven, where it remained for five minutes until the supernatant liquid turned into colorless. After pouring the remaining mixture into a furnace-placed stainless steel pan and heating it for eight hours at 70 °C, the black cake was pulverized, and the composite catalyst was evenly obtained and designated as m-SMC(Equation 1). To provide a comparison, 5 mL of hydrazine was used to chemically reduce silver permanganate at room temperature. The solution was stirred for 24 hours until the supernatant liquid was colorless. The product that was designated as c-SMC (Equation 2).The procession of reaction follows the listed equation.

$$AgMnO_4 \rightarrow Ag + MnO_2 + O_2 \tag{8}$$

$$AgMnO_4 + N_2H_4 \rightarrow Ag + MnO_2 + 2H_2O + N_2 \tag{9}$$

3.2. Preparation of electrolyte, electrodes and assembly of solid-state Zinc-air cell

When making the alkaline polymer gel electrolyte (GPE), we followed the procedures outlined in the literature[38]. In a beaker at room temperature, one gram of poly(vinyl alcohol)(PVA) was added to a 6 mol·L^{-1} KOH aqueous solution and stirred. The initial gel could be kept in an airtight glass container for more than 70 hours at 25 °C to prevent carbon dioxide absorption and water evaporation. Gas bubbles were eliminated under vacuum once the gel was formed. The resultant gel was stored at 25 °C for future use.

 doi:10.20944/preprints202401.0200.v1

To make air electrodes, two-layer gas diffusion electrode was built, with one layer referred to as the catalyst layer or active layer. The other is known as the air layer or hydrophobic layer. The air layer consists of CNTs, Na_2SO_4 and poly-tetrafluoroethylene (PTFE, from Aldrich) with weight ratio of 2:1:7. These chemicals were combined with ethanol to create a dough that was then rolled over a porous nickel substrate. A 6:2:3 weight ratio mixture of the catalyst, Na_2SO_4, and PTFE was first combined and crushed in excess ethanol. After that, it was rolled into a sheet with a thickness of 0.1 to 0.4 millimeters and a circular shape of 20 millimeters. Then, it was pressed for five minutes at a pressure of 3×10^7 kg·cm^{-2} onto the air layer that had already been prepared. Subsequent to drying and heat treatment at 40 °C for half hour, the final electrode is normally 0.2 $\sim$ 0.5 mm of thickness. In the electrochemical experiments, testing cells with a catalytic air electrode as the cathode, zinc powder as the anode, and an alkaline PVA gel polymer electrolyte (GPE) were constructed.

3.3. Measurements

Morphologies of the SMC composite catalyst were observed with scanning electron microscope (SEM) (Leo-1430 VP), transmission electron microscope (TEM). The composition and structure of SMC were also examined by energy dispersion spectrometer (EDS) and X-ray diffraction (XRD). The CHI 760E electrochemical workstation system (CHI Instrument) was used to perform the air electrode's polarization characteristic. Measurements were acted in a three-terminal cell with the air cathode as the working anode, Hg/HgO as the reference electrode and a platinum foil as the counter cathode. A 6 mol·L^{-1} KOH aqueous solution was used as electrolyte. The discharge characteristic of the solid-state zinc-air cell was tested with galvanostatic charge-discharge unit (8-channel Battery analyzer). Resistance, open circuit potentials of ZABs were recorded by a CHI760 E electrochemical workstation.

4. Conclusion

A dual-functional silver-manganese dioxide-CNTs (SMC) ternary composite catalyst was obtained successfully via simply one-step microwave heating silver permanganate. We explored the electrolytic activity of catalyst for ORR in alkaline condition and the discharge performance of solid-state zinc-air cell with SMC. Morphology and composition analysis indicate that silver and alpha manganese dioxide have been produced during microwave irradiation, and anchored uniformly on CNTs. Polarization of air electrode with SMC catalyst and discharge of solid-state zinc-air cell coincidently reveal that the dual-functional ternary m-SMC composite catalyst has higher activity for ORR and better cell performance than the c-SMC. The improvement of zinc-air cell performance is attributed to a synergetic outcome of silver and alpha manganese dioxide.

Author Contributions: Conceptualization, Guoqing.Zhang, Tuanwu.Cao, and Binbin.Jin.; methodology, Guoqing.Zhang.; software, Guoqing.Zhang.; validation, Peng.Zhang.; formal analysis, Tuanwu.Cao.; investigation, Shuying.Kong.; data curation, Shuying.Kong.; writing—original draft preparation, Guoqing.Zhang.; writing—review and editing, Guoqing.Zhang.; visualization, Shuying.Kong.; supervision, Guoqing.Zhang.; project administration, Guoqing.Zhang.; funding acquisition, Guoqing.Zhang. All authors have read and agreed to the published version of the manuscript.

Funding: This research was funded by National Foundation of Science of China grant number 21443004, and by the 47th (1792) Scientific Research Foundation for the Returned Overseas Chinese Scholars; by the Chunhui Program of Ministry of Education of China (Z2014083, Z2014084).

Data Availability Statement: The data presented in this study are available within the article. We are working to make the codes underlying this study available on Github.

Conflicts of Interest: The authors declare no conflict of interest.

References

1. Zhu, J.; Xiao, M.; Zhang, Y.; Jin, Z.; Peng, Z.; Liu, C.; Chen, S.; Ge, J.; Xing, W. Metal-Organic Framework-Induced Synthesis of Ultrasmall Encased NiFe Nanoparticles Coupling with Graphene as an Efficient Oxygen Electrode for a Rechargeable Zn-Air Battery. *ACS Catalysis* **2016**, *6*, 6335–6342. doi:10.1021/acscatal.6b01503.
2. Zhu, X.; Hu, C.; Amal, R.; Dai, L.; Lu, X. Heteroatom-doped carbon catalysts for zinc-air batteries: progress, mechanism, and opportunities. *Energy & Environmental Science* **2020**, *13*, 4536–4563. doi:10.1039/d0ee02800b.
3. Rahman, M.A.; Wang, X.; Wen, C. High Energy Density Metal-Air Batteries: A Review. *Journal of The Electrochemical Society* **2013**, *160*, A1759–A1771. doi:10.1149/2.062310jes.
4. Watanabe, M.; Tryk, D.A.; Wakisaka, M.; Yano, H.; Uchida, H. Overview of recent developments in oxygen reduction electrocatalysis. *Electrochimica Acta* **2012**, *84*, 187–201. doi:10.1016/j.electacta.2012.04.035.
5. Yang, D.; Zhang, L.; Yan, X.; Yao, X. Recent progress in oxygen electrocatalysts. *Small Methods* **2017**, *11*, 1700209. doi:doi:10.1002/smtd.201700209.
6. Zhu, C.; Li, H.; Fu, S.; Du, D.; Lin, Y. Highly efficient nonprecious metal catalysts towards oxygen reduction reaction based on three-dimensional porous carbon nanostructures. *Chemical Society Reviews* **2016**, *45*, 517–531. doi:10.1039/c5cs00670h.
7. Xia, B.Y.; Yan, Y.; Li, N.; Wu, H.B.; Lou, X.D.; Wang, X. A metal-organic framework-derived. *Nature Energy* **2016**, *1*, 15006. doi:doi:10.1038/ nenergy.2015.6.
8. Tiwari, J.N.; Nath, K.; Kumar, S.; Tiwari, R.N.; Kemp, K.C.; Le, N.H.; Youn, D.H.; Lee, J.S.; Kim, K.S. Stable platinum nanoclusters on genomic DNA-graphene oxide with a high oxygen reduction reaction activity. *Nature Communications* **2013**, *4*. doi:10.1038/ncomms3221.
9. Nesselberger, M.; Roefzaad, M.; Fayçal Hamou, R.; Ulrich Biedermann, P.; Schweinberger, F.F.; Kunz, S.; Schloegl, K.; Wiberg, G.K.H.; Ashton, S.; Heiz, U.; Mayrhofer, K.J.J.; Arenz, M. The effect of particle proximity on the oxygen reduction rate of size-selected platinum clusters. *Nature Materials* **2013**, *12*, 919–924. doi:10.1038/nmat3712.
10. Wang, H.F.; Tang, C.; Zhang, Q. A Review of Precious-Metal-Free Bifunctional Oxygen Electrocatalysts: Rational Design and Applications in Zn-Air Batteries. *Advanced Functional Materials* **2018**, *28*, 1803329. doi:10.1002/adfm.201803329.
11. Zeng, K.; Zheng, X.; Li, C.; Yan, J.; Tian, J.; Jin, C.; Strasser, P.; Yang, R. Recent Advances in Non-Noble Bifunctional Oxygen Electrocatalysts toward Large-Scale Production. *Advanced Functional Materials* **2020**, *30*, 2000503. doi:10.1002/adfm.202000503.
12. Qaseem, A.; Chen, F.; Wu, X.; Johnston, R.L. Pt-free silver nanoalloy electrocatalysts for oxygen reduction reaction in alkaline media. *Catalysis Science & Technology* **2016**, *6*, 3317–3340. doi:10.1039/c5cy02270c.
13. Sun, H.; Hu, Z.; Yao, C.; Yu, J.; Du, Z. Silver Doped Amorphous MnO_2 as Electrocatalysts for Oxygen Reduction Reaction in Al-Air Battery. *Journal of The Electrochemical Society* **2020**, *167*, 080539. doi:10.1149/1945-7111/ab91c7.
14. Poudel, M.B.; Shin, M.; Kim, H.J. Polyaniline-silver-manganese dioxide nanorod ternary composite for asymmetric supercapacitor with remarkable electrochemical performance. *International Journal of Hydrogen Energy* **2021**, *46*, 474–485. doi:10.1016/j.ijhydene.2020.09.213.
15. Tarasevich, M.R.; Sadkowski, A.; Yeager, E. Oxygen Electrochemistry, 1983.
16. Wong, E.W.; Sheehan, P.E.; Lieber, C.M. Nanobeam Mechanics: Elasticity, Strength, and Toughness of Nanorods and Nanotubes. *Science* **1997**, *277*, 1971–1975. doi:10.1126/science.277.5334.1971.
17. Tans, S.J.; Verschueren, A.R.M.; Dekker, C. Room-temperature transistor based on a single carbon nanotube. *Nature* **1998**, *393*, 49–52. doi:10.1038/29954.
18. Planeix, J.M.; Coustel, N.; Coq, B.; Brotons, V.; Kumbhar, P.S.; Dutartre, R.; Geneste, P.; Bernier, P.; Ajayan, P.M. Application of Carbon Nanotubes as Supports in Heterogeneous Catalysis. *Journal of the American Chemical Society* **1994**, *116*, 7935–7936. doi:10.1021/ja00096a076.
19. Jin, Y.; Chen, F.; Lei, Y.; Wu, X. A Silver-Copper Alloy as an Oxygen Reduction Electrocatalyst for an Advanced Zinc-Air Battery. *ChemCatChem* **2015**, *7*, 2377–2383. doi:10.1002/cctc.201500228.
20. Dembinska, B.; Brzozowska, K.; Szwed, A.; Miecznikowski, K.; Negro, E.; Di Noto, V.; Kulesza, P.J. Electrocatalytic Oxygen Reduction in Alkaline Medium at Graphene-Supported Silver-Iron Carbon Nitride

Sites Generated During Thermal Decomposition of Silver Hexacyanoferrate. *Electrocatalysis* **2018**, *10*, 112–124. doi:10.1007/s12678-018-0501-3.

21. Sun, J.; Guo, N.; Song, T.; Hao, Y.R.; Sun, J.; Xue, H.; Wang, Q. Revealing the interfacial electron modulation effect of CoFe alloys with CoC encapsulated in N-doped CNTs for superior oxygen reduction. *Advanced Powder Materials* **2022**, *1*, 100023. doi:10.1016/j.apmate.2021.11.009.
22. Li, P.C.; Hu, C.C.; Noda, H.; Habazaki, H. Synthesis and characterization of carbon black/manganese oxide air cathodes for zinc-air batteries: Effects of the crystalline structure of manganese oxides. *Journal of Power Sources* **2015**, *298*, 102–113. doi:10.1016/j.jpowsour.2015.08.051.
23. Rao, K.J.; Vaidhyanathan, B.; Ganguli, M.; Ramakrishnan, P.A. Synthesis of Inorganic Solids Using Microwaves. *Chemistry of Materials* **1999**, *11*, 882–895. doi:10.1021/cm9803859.
24. Liu, J.; Liu, J.; Song, W.; Wang, F.; Song, Y. The role of electronic interaction in the use of Ag and Mn_3O_4 hybrid nanocrystals covalently coupled with carbon as advanced oxygen reduction electrocatalysts. *J. Mater. Chem. A* **2014**, *2*, 17477–17488. doi:10.1039/c4ta03937h.
25. Khilari, S.; Pandit, S.; Ghangrekar, M.M.; Das, D.; Pradhan, D. Graphene supported α-MnO_2 nanotubes as a cathode catalyst for improved power generation and wastewater treatment in single-chambered microbial fuel cells. *RSC Advances* **2013**, *3*, 7902. doi:10.1039/c3ra22569k.
26. Ge, X.; Sumboja, A.; Wuu, D.; An, T.; Li, B.; Goh, F.W.T.; Hor, T.S.A.; Zong, Y.; Liu, Z. Oxygen Reduction in Alkaline Media: From Mechanisms to Recent Advances of Catalysts. *ACS Catalysis* **2015**, *5*, 4643–4667. doi:10.1021/acscatal.5b00524.
27. Park, S.A.; Lee, E.K.; Song, H.; Kim, Y.T. Bifunctional enhancement of oxygen reduction reaction activity on Ag catalysts due to water activation on $LaMnO_3$ supports in alkaline media. *Scientific Reports* **2015**, *5*. doi:10.1038/srep13552.
28. Spendelow, J.S.; Wieckowski, A. Electrocatalysis of oxygen reduction and small alcohol oxidation in alkaline media. *Physical Chemistry Chemical Physics* **2007**, *9*, 2654. doi:10.1039/b703315j.
29. Kinoshita, K. Carbon: electrochemical and physicochemical properties. *www.osti.gov* **1988**.
30. Linden, D.; Reddy, T.B. *Handbook of batteries*; Mcgraw-Hill, 2002.
31. Cao, R.; Lee, J.S.; Liu, M.; Cho, J. Recent Progress in Non-Precious Catalysts for Metal-Air Batteries. *Advanced Energy Materials* **2012**, *2*, 816–829. doi:10.1002/aenm.201200013.
32. Slanac, D.A.; Lie, A.; Paulson, J.A.; Stevenson, K.J.; Johnston, K.P. Bifunctional Catalysts for Alkaline Oxygen Reduction Reaction via Promotion of Ligand and Ensemble Effects at Ag/MnO_x Nanodomains. *The Journal of Physical Chemistry C* **2012**, *116*, 11032–11039. doi:10.1021/jp3012816.
33. Cao, Y.L.; Yang, H.X.; Ai, X.P.; Xiao, L.F. The mechanism of oxygen reduction on MnO_2-catalyzed air cathode in alkaline solution **2003**. *557*, 127–134. doi:doi:10.1016/ s0022-0728(03)00355-3.
34. Goh, F.T.; Liu, Z.; Ge, X.; Zong, Y.; Du, G.; Hor, T.A. Ag nanoparticle-modified MnO_2 nanorods catalyst for use as an air electrode in zinc-air battery. *Electrochimica Acta* **2013**, *114*, 598–604. doi:10.1016/j.electacta.2013.10.116.
35. Li, P.C.; Hu, C.C.; Lee, T.C.; Chang, W.S.; Wang, T.H. Synthesis and characterization of carbon black/manganese oxide air cathodes for zinc-air batteries. *Journal of Power Sources* **2014**, *269*, 88–97. doi:10.1016/j.jpowsour.2014.06.108.
36. Hu, J.; Shi, Z.; Wang, X.; Qiao, H.; Huang, H. Silver-modified porous 3D nitrogen-doped graphene aerogel: Highly efficient oxygen reduction electrocatalyst for Zn-Air battery. *Electrochimica Acta* **2019**, *302*, 216–224. doi:10.1016/j.electacta.2019.02.051.
37. Rao, C.S.; Gunasekaran, G. Cobalt-Lead-Manganese oxides combined cathode catalyst for air electrode in Zinc-air battery. *Electrochimica Acta* **2015**, *176*, 649–656. doi:10.1016/j.electacta.2015.07.056.
38. Lewandowski, A.; Skorupska, K.; Malinska, J. Novel poly(vinyl alcohol)-KOH-H_2O alkaline polymer electrolyte. *Solid State Ionics* **2000**, *13*. doi:doi:https://doi.org/10.1016/S0167-2738(00) 00733-5.